Journal of Materials Chemistry C

PAPER

Cite this: J. Mater. Chem. C, 2014, 2, 9941

An extremely rapid dip-coating method for self-assembly of octadecylphosphonic acid and its thermal stability on an aluminum film

Donghan Chen,[b] Horace King Yin Wu,[a] Soheila Naderi-Gohar,[ac] Yiliang Wu,[d] Yining Huang[b] and Heng-Yong Nie*[ac]

We introduce a dip-coating method for preparing self-assembled monolayers (SAMs) of octadecylphosphonic acid (OPA) on hydrophilic substrates by selecting anisole (methoxybenzene) as the solvent, which has a dielectric constant of 4.3. We demonstrate that full-coverage OPA SAMs are formed in a couple of seconds on a cleaved mica substrate upon its dipping in a 1 mM OPA solution in anisole. In order to develop applications of this extremely rapid coating approach in surface engineering, we investigate the thermal stability of OPA SAMs dip-coated on a UV/ozone-cleaned aluminum film using water contact angle measurements and time-of-flight secondary ion mass spectrometry. It was clarified that the OPA SAMs annealed in air at up to 200 °C exhibited excellent hydrophobicity and the degradation mechanism is oxidation of the alkyl chains.

Received 9th September 2014
Accepted 7th October 2014

DOI: 10.1039/c4tc02017k

www.rsc.org/MaterialsC

1. Introduction

Self-assembled monolayers (SAMs) of amphiphilic organic molecules formed on a solid surface have generated an enormous amount of interest in interdisciplinary research areas as diverse as molecular engineering of surfaces, tribology, biology, nanotechnology, polymer composites, organic electronics and analytical chemistry.[1–3] The mechanism for SAM formation is that molecular headgroups are adsorbed on the substrate immersed in a solution of molecules of interest, followed by a slower process of proper orientation of the molecular chains. To obtain the final SAMs, it is common to immerse the substrate in the solution for several hours followed by copiously rinsing the surface to remove excess molecules residing on the monolayers.[1–4] SAMs of organophosphonic acid, especially octadecylphosphonic acid (OPA), have long been used to modify the surface of aluminum (Al) for lubrication and anti-corrosion.[5] This system relies on the ease of formation of the robust P–O–Al linkage as a result of the condensation reaction between its hydroxyl groups and the surface hydroxyl groups on the (native) oxide layer of Al films.[6]

More recently, the interest of using OPA SAMs to modify surface/interface properties is rapidly growing.[7–9] Especially, applications of OPA SAMs in enhancing the compatibility between organic and inorganic materials, as well as controlling electronic properties in organic electronic devices have expanded enormously.[9–15] For example, OPA SAMs between an aluminum oxide dielectric and organic semiconductor enhance the organic transistor performance (increased charge carrier mobility and reduced leak current).[14,15] As OPA molecules bond more strongly to some metal oxides than others, OPA SAMs have very recently been used in metal–dielectric[16] and metal–metal[17] patterning, in which the chemistry of the molecular headgroup and the substrate plays the most important role.

The vast majority of the OPA SAMs were prepared using polar solvents such as alcohols. The common practice is to immerse the substrate in an OPA solution for hours or even days, after which rinse is necessary to remove excessive molecules from residing on the monolayer. Taking the example of OPA SAMs on mica, this monolayer preparation method is unlikely to provide full-coverage monolayers even after an immersion time of four days.[18] With the rapid development of applications of OPA SAMs in, for example, organic electronic devices, there is an urgent need to develop a more rapid SAM formation approach rendering higher quality monolayers.[19] We have shown that using a nonpolar solvent such as chloroform or trichloroethylene allows spin-coating of OPA SAMs on various hydrophilic surfaces.[20] The mechanism behind this is attributed to the concentration of OPA headgroups on the medium surface as a consequence of these two solvents having dielectric constants of 3.4 and 4.8. In order to harness the unique interaction between OPA molecules and a solvent having a dielectric constant of ~4,

[a]Surface Science Western, The University of Western Ontario, 999 Collip Circle, London, N6G 0J3, Ontario, Canada. E-mail: hnie@uwo.ca
[b]Department of Chemistry, The University of Western Ontario, London, N6A 5B7, Ontario, Canada
[c]Department of Physics and Astronomy, The University of Western Ontario, London, N6A 3K7, Ontario, Canada
[d]Advanced Materials Laboratory, Xerox Research Centre of Canada, 2660 Speakman Dr., Mississauga, L5K 2L1, ON, Canada

we show that by using anisole as the solvent for OPA molecules one achieves full-coverage OPA SAMs on a hydrophilic substrate by dip-coating in a matter of seconds. This extremely rapid dip-coating method is due to the fact that anisole has a dielectric constant of 4.3. However, unlike the previously utilized chlorine-containing solvents such as chloroform and trichloroethylene, anisole is a more environmentally benign solvent.[21]

In order to demonstrate the efficacy of this dip-coating approach, we use cleaved mica (because of its atomically flat surface) to verify the coverage of OPA SAMs using an atomic force microscope (AFM). Since OPA SAMs on the Al surface are perhaps the most studied system, we use water contact angle (CA)[22] and time-of-flight secondary ion mass spectrometry (TOF-SIMS)[23] to investigate the hydrophobicity and the thermal stability of the OPA SAMs dip-coated on an Al film and their degradation mechanism upon annealing in air at elevated temperatures. CAs are sensitive to alternations that impact the surface chemistry[22] and TOF-SIMS is a surface sensitive technique to capture chemical information within the topmost 1–2 monolayers.[23,24] Therefore, these two surface-sensitive techniques are especially useful in probing the surface chemistry of SAMs.[22,25,26] It has also been demonstrated that TOF-SIMS is uniquely suited to differentiate intact OPA molecules from those altered in any ways, which no longer have a chance to be fragmented as a deprotonated molecular ion.[27]

2. Experimental

OPA [$CH_3(CH_2)_{17}P(=O)(OH)_2$] was purchased from Alfa Aesar (97% purity, Ward Hill, MA). The melting point of (crystalline powder of) OPA is ~98 °C. Prior to use, the OPA powder was heated in a glass bottle to ~100 °C for ~5 min in order to remove moisture adsorbed in the powder. Then anisole was poured into the bottle to dissolve OPA molecules – such a solution of OPA and anisole is referred to as "OPA solution in anisole" in this article. OPA solutions in anisole having different concentrations were made and kept at ~60 °C for our dip-coating experiment. A 50 nm thick Al film was coated on a Si (100) substrate by radio frequency magnetron-sputtering, which was cut into small pieces and used for the dip-coating experiment.

The Al-coated substrates were cleaned with methanol followed by exposure to UV light (with irradiation at 184.9 and 253.7 nm) in a chamber in the presence of ozone for 40 min. The UV/ozone-treated substrates were dipped into and quickly withdrawn from OPA solutions in anisole having concentrations ranging from 0 to 1 mM. This experiment was to determine the minimum OPA solution concentration for achieving full-coverage for dip-coating. We stress that the dip-coating process lasted only for 2–3 s, after which there were no further treatments (*e.g.*, rinse) done. In order to conduct a thermal stability study, 16 samples were made by dip-coating the substrate using a 1 mM OPA solution in anisole (denoted as OPA/Al), with two samples used as the control and 14 used for the annealing experiment. Then two samples each were annealed for 15 min on a hot plate (in air) set at 100, 150, 200, 250, 300, 350 and 400 °C, respectively. CAs were measured on one set of the control and annealed samples at 3–5 spots after they cooled naturally to room temperature using a contact angle goniometer (Ramé-Hart's Model 100-00) using a sessile de-ionized water drop. Another set of the control and annealed samples were subjected to TOF-SIMS analysis.

An ION-TOF (GmbH) TOF-SIMS IV equipped with a Bi liquid metal ion gun was employed to investigate the control and annealed OPA/Al samples. A pulsed 25 keV Bi_3^+ cluster primary ion beam (with a pulse width of ~1 ns and a target current of ~1 pA) was used to bombard the sample surface to generate secondary ions. The secondary ions, either positive or negative at a time, were extracted by an electric field (2 kV), mass separated and detected *via* a reflectron-type of the time-of-flight analyzing system. The cycle time for the processes of the bombardment of the primary ion beam and the detection of the secondary ions was 100 μs. A pulsed, low energy (~18 eV) electron flood was used to neutralize sample charging; the current was maintained below ~20 μA maximum to avoid sample damage. The base pressure of the analytical chamber was $<1 \times 10^{-8}$ mbar. For each sample, negative and positive secondary ion mass spectra were collected on three spots from 128 × 128 pixels over an area of 500 μm × 500 μm, which were calibrated using ion species of H^- and PO_3^-, and H^+ and $C_3H_5^+$, respectively. The mass resolution for ion fragments of C_2H^-, PO_3^-, $C_2H_5^+$ and $C_3H_7^+$ was 2800, 4600, 3200 and 4100, respectively.

The target current of ~1 pA generated by the pulsed primary ion beam bombardment resulted in ~600 ions per shot. Each spectrum was collected with the primary ion beam bombarding the sample surface with $\sim 6 \times 10^5$ shots over 128 × 128 pixels in an area of 500 μm × 500 μm. This resulted in a primary ion dosage of $\sim 1.5 \times 10^{11}$ cm^{-2}. This dosage was within the static limit[28] since it was less than 0.04% of the molecular density (4×10^{14} cm^{-2}) of an OPA monolayer.[18] In order to compare changes in the intensities of ion fragments obtained on samples annealed at different temperatures, Poisson-correction was applied for the dead time effect of the detection system.[29] Such corrected intensities of ion fragments are normalized to the total ion intensity.

The dynamic force mode of a Park Systems XE-100 AFM was used to image the morphology of OPA SAMs dip-coated on cleaved mica, which is an atomically flat surface, allowing one to unambiguously image the coverage of the monolayer. In this mode, a cantilever with a nominal spring constant of 40 N m^{-1} and a resonant frequency of 300 kHz (T300, Vistaprobes) was vibrated and its reduced amplitude was used as the feedback parameter to image the surface morphology. The nominal tip radius of the cantilever we used was approximately 10 nm. The AFM scanner was calibrated using a calibration grating (TGZ1_PTB from NT-MDT) having a step height of 21.9 ± 0.8 nm and a pitch size of 3 ± 0.01 μm. The AFM images with a pixel density of 256 × 256 were obtained in an area of 2 μm × 2 μm at a scan rate of 1 Hz (*i.e.*, a tip velocity of 2 μm s^{-1}) in air under a relative humidity of 40%.

3. Results and discussion

Shown in Fig. 1 are advancing, static and receding CAs measured on OPA/Al samples made by dipping Al-coated Si

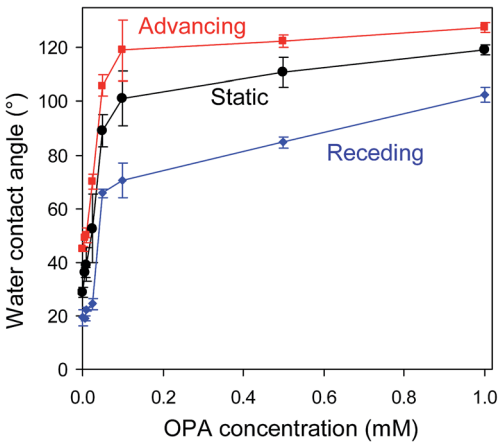

Fig. 1 Water contact angles measured on OPA/Al samples as a function of OPA concentration solution in anisole, in which the Al films were dipped for 2–3 s.

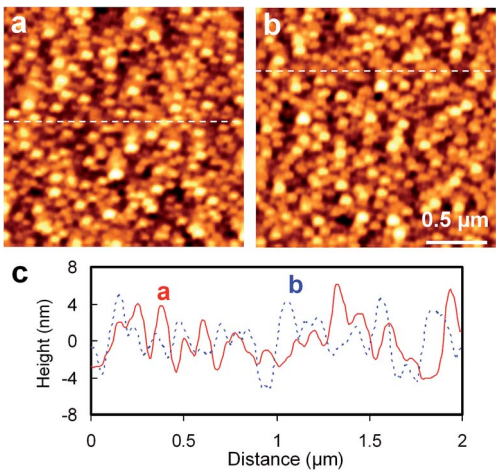

Fig. 2 Topographic images obtained in an area of 2 μm × 2 μm on the surface of (a) a bare Al film and (b) OPA SAMs dip-coated on an Al film using a 1 mM OPA solution in anisole. The profiles a (solid line) and b (broken line) shown in (c) are isolated from the AFM images (indicated by the broken lines) in (a) and (b), respectively. The height scale for (a) and (b) is 23.0 and 25.0 nm, respectively.

substrates into OPA solutions in anisole having different concentrations ranging from 0 to 1 mM. This experiment was carried out to determine the minimum concentration that ensures an excellent coverage of OPA SAMs. We first look at the static CAs of the OPA/Al samples as a function of solution concentration. Then we discuss the observed contact angle hysteresis (CAH), which is the difference between the advancing and receding CAs.

Static CAs measured on OPA/Al samples increased rapidly with an increasing concentration of OPA solution from 0 to 0.05 mM, reaching ~90°. They kept increasing with a slower pace at further increased OPA concentrations from 0.1 to 1 mM. We noticed that an Al film dipped into a higher concentration solution became dry when being withdrawn from the solution, which is a reflection that the Al film became hydrophobic upon dipping. As shown in Fig. 1, with a 1 mM OPA solution, we were able to make an OPA/Al sample having CAs reaching 120°, which is a sign that the surface is covered by close-packed OPA molecules. Therefore, we conclude that 1 mM is a large enough concentration of an OPA solution to allow one to dip-coat a good quality OPA monolayer on an Al film. We stress that the dip-coating required only a couple of seconds and no further steps (such as rinse) were needed.

The contact angle hysteresis (CAH) observed on the OPA/Al sample made with the 1 mM OPA solution in anisole is approximately 30°. It has been reported that CAH may be affected by surface roughness and chemical heterogeneity.[30,31] In order to estimate the roughness of the Al film AFM was used to image the surface morphology of a bare Al film and an OPA/Al sample dip-coated in a 1 mM OPA solution. The AFM images in Fig. 2a and b show no significant morphological differences between the bare and OPA-coated Al films, from which the surface has a root mean square roughness of 2.8 and 3.1 nm, respectively. Two profiles each isolated from the AFM images in Fig. 2a and b are plotted in Fig. 2c, showing that the corrugation for both samples is approximately 10 nm. Therefore, the Al film is relatively rough in comparison with the thickness of OPA SAMs (~2 nm). The Al film used in this study has a thickness of 50 nm, resulting in a much rougher surface than the Al film used in a previous study,[20] which had a thickness of 10 nm and a root mean square roughness of only 0.3 nm. The CAH for a full-coverage OPA monolayer formed on such a smoother Al film was approximately 19°.[20]

The chemical heterogeneity in our case is related to the coverage of the OPA SAMs, that is, if the coverage is not 100%, then we have both the hydrophobic methyl-terminated OPA SAMs and exposed hydrophilic aluminum oxide spots. If this were the case, then the cleaning process for Al films using UV/O would be optimized. Though we can qualitatively explain the CAH observed for our dip-coated OPA SAMs by considering the roughness and/or plausibly the coverage of the monolayer, it is worth pointing out that even for a flat surface with chemical homogeneity, such as octadecanethiol SAMs on a molecularly smooth GaAs surface, CAH still exists.[32] This is essentially due to energy dissipation for a water droplet being placed on the monolayer surface, to which the droplet imposes chemical interactions as well as mechanical deformation of the monolayer.

The roughness of the Al film used in this study prevented AFM studies on the coverage of OPA SAMs. In order to investigate the coverage of the OPA monolayer, we selected cleaved mica as the substrate, which is atomically flat and any uncovered surface or any multilayers would be easily visualized by the height difference. Shown in Fig. 3a is an AFM image obtained on a sample made by dip-coating cleave mica into a 0.01 mM OPA solution. In such a dilute solution only sparse islands of OPA molecules were formed on the cleaved mica surface. With an increased concentration of 0.1 mM, as clearly shown in Fig. 3b, much denser islands were formed. The shorter islands are 1.0 to 1.3 nm, suggesting that the OPA molecules in these islands were not yet close-packed. On the other hand, the height

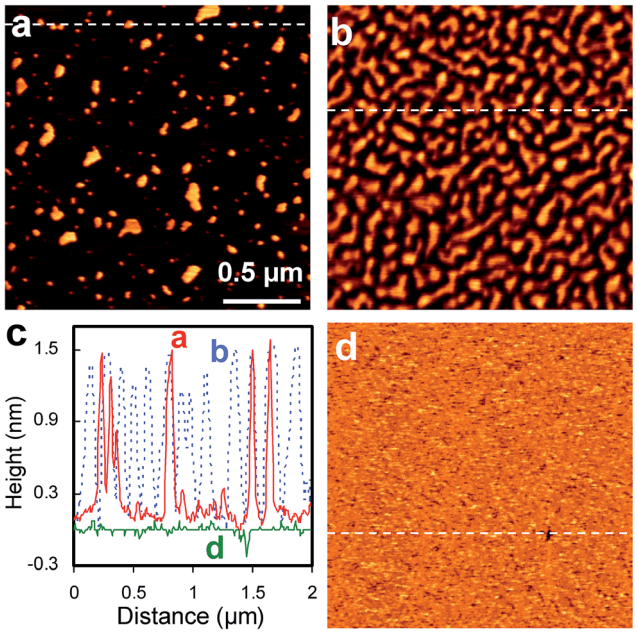

Fig. 3 Topographic images obtained in an area of 2 μm × 2 μm on the surface of OPA SAMs dip-coated on cleaved mica using a (a) 0.01 mM and (b) 0.1 mM OPA solution in anisole, respectively. The profiles a (solid line), b (broken line) and d (solid line) shown in (c) are isolated from the AFM images (indicated by the broken lines) in (a), (b) and (d), respectively. Full-coverage OPA SAMs were obtained on cleaved mica using a 1 mM OPA solution in anisole. The height scale for (a), (b) and (d) is 2.1, 2.3 and 0.4 nm, respectively.

of the tallest islands shown in Fig. 3b was estimated to be 1.7 ± 0.1 nm, which is in agreement with the reported thickness of OPA SAMs prepared on cleaved mica using other methods.[18,20] However, as indicated by profiles a and b in Fig. 3c, which are isolated from the AFM images in Fig. 3a and b, respectively, many OPA islands have a height reaching approximately 1.5 nm. When the OPA concentration was increased to 1 mM, as shown in Fig. 3d, a full-coverage OPA monolayer was formed, resulting in a roughness of merely 0.03 nm, which is similar to that of a cleaved mica surface. Profile d in Fig. 3c is isolated from the AFM image in Fig. 3d, showing that the corrugation of the monolayer surface is on the order of 0.1 nm. We constantly achieved hexadecane contact angles of 45–47° on samples dip-coated in 1 mM OPA solutions in anisole, which confirmed that the formation of full-coverage OPA SAMs since hexadecane is known to make a contact angle of ~46° on methyl group terminated SAMs.[20,33]

The coverage estimated from the AFM images of OPA SAMs achieved by dip-coating using OPA solutions having a concentration of 0.01 (Fig. 3a) and 0.1 mM (Fig. 3b) is approximately 10% and 60%, respectively. Because we could not detect the coverage of OPA SAMs on the Al film due to its roughness, we try to have an idea as how coverage is related to the water CA by assuming that the coverage of OPA formed on the Al film would be comparable to that on mica upon dip-coating using the same OPA solution. Then according to Fig. 1, which shows water CAs of OPA SAMs on the Al films as a function of OPA concentration, 10% coverage OPA SAMs (or an OPA density of 4×10^{13} cm^{-2}) would have a static CA of ~40°. Similarly, 60% coverage (2.4×10^{14} cm^{-2}) and full-coverage (4×10^{14} cm^{-2})[18] OPA SAMs would have a contact angle of 100° and 120°, respectively. The above arguments should serve as a crude clue as how OPA coverage impacts water CAs. However, because coverage of OPA SAMs on mica may deviate from that on the Al film, future studies using Al films being smooth enough to allow OPA SAM coverage estimation using AFM are expected to provide more accurate results on clarifying this important issue of coverage *vs.* water CA.

It is worth noting that for the particular case in the OPA SAM formation on cleaved mica when a polar solvent was used, such as isopropyl alcohol, it has proven impossible to form full-coverage OPA SMAs on cleaved mica even when the substrate was immersed in the solution for days.[18] In contrast, we have shown in Fig. 3d that dipping cleaved mica in a 1 mM OPA solution in anisole, in a matter of a couple of seconds, renders full coverage OPA SAMs. Here we discuss the mechanism as why such rapid formation of SAMs becomes possible. An apparent difference between polar and nonpolar solvents lies in their different dielectric constants (DCs). Solvent DC is a measure of its ability to separate or dissolve charged particles, which is an important factor in controlling chemical reactions taking place in a solution.[34,35] Polar solvents have a higher DC, such as ethanol (DC is 24.3) and tetrahydrofuran (7.6). They dissolve amphiphilic molecules (*i.e.*, having a polar headgroup and a non-polar tail) much better than non-polar solvents do, which is the reason why polar solvents have been selected by most researchers for their work on SAM preparation. When a polar solvent is used, the amphiphilic molecules in the solution are well-dispersed and become adsorbed on the substrate. With more molecules continue to be adsorbed, they eventually form closely packed monolayers *via* van der Waals forces between the molecular chains.[4] In most cases, immersion times are from a couple of hours to a couple of days. Because the molecules are well dispersed in the solution, it is inevitable that excessive molecules are present on the monolayer formed. Rinse is thus required to remove the excessive molecules to obtain the final SAM product.[1–4]

On the other hand, OPA molecules are only sparsely dissolved in nonpolar solvents having smaller DCs, which is the reason why the OPA solution used in this study was kept at 60 °C (so that the molecules would be fully dissolved in the solvent). Examples of nonpolar solvents are chloroform (4.8), anisole (4.3) and trichloroethylene (3.4). However, these solvents act as an active medium to concentrate and align the polar headgroups of the amphiphilic molecules on their surface so that the molecules are in a state to seek hydrophilic entities.[20] The only requirement in this method for OPA SAM formation on a hydrophilic surface is the physical contact between the medium and the substrate. As illustrated in Fig. 4, when a hydrophilic substrate is inserted into the solution, the polar OPA headgroups are forced to align on the newly created interface, while the nonpolar alkyl chains are left in the medium. The concentration of OPA headgroups on the medium surface lowers the activation energy for the molecules to be transferred onto the hydrophilic substrate. This unique property of OPA solution in a

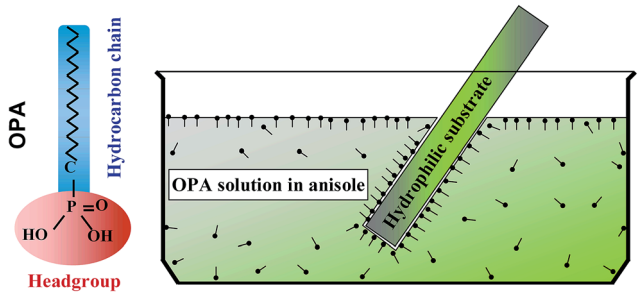

Fig. 4 Schematic illustration of an OPA molecule and the dip-coating method using a solvent having a dielectric constant of ~4, which drives the polar OPA headgroups to the interface generated between the solution and a hydrophilic surface (or air).

solvent having a DC of ~4 facilitates an extremely fast growth of SAMs. However, for nonpolar solvents having a DC much smaller than 4, such as hexane (1.9), OPA molecules will form inverted micelles, thus unable to render OPA monolayers on a hydrophilic substrate.[20]

It is worth noting that the monolayer formation mechanism in our method only requires a substrate that is hydrophilic (or has high surface energy) because the headgroups of OPA molecules in anisole are forced to align on the medium surface, seeking a hydrophilic entity to transfer to. Therefore, our method is non-substrate specific and is expected to be able to apply to various metal oxides, as long as the surface to be modified is hydrophilic.

Our method shows some similarity to the Langmuir–Blodgett (LB) film approach, in which the amphiphilic molecules are squeezed to form a single Langmuir monolayer on the subphase surface (water) in a trough.[36] A single layer LB film or a multilayer LB film will be deposited onto a substrate, depending on the times the substrate passes through the Langmuir monolayer at the air/water interface. However, there are two fundamental differences between the two methods. First, the non-polar tails face outward to air in the Langmuir monolayer, while in our method the polar headgroups are on the medium surface and face outward to air. Second, there is only a single Langmuir monolayer available in the trough. By contrast, in our method, whenever the molecules aligned on the medium surface are used for monolayer formation onto a hydrophilic substrate, molecules inside the medium will immediately occupy the medium surface so long as the concentration of molecules is large enough.

The concentration of the polar headgroups of OPA on the solution surface renders a decrease in activation energy for transfer of these aligned molecules onto a high surface energy substrate, which is the physics behind this immense difference in formation mechanisms of OPA monolayers caused solely by choosing nonpolar solvents having a DC of ~4. There have been developments of gas phase approaches to form monolayers since a solvent typically plays a negative role in many cases.[16] Our results, however, demonstrate that by harnessing the interactions between OPA headgroups and a solvent having a DC of ~4, a solvent can actually play an essential role in lowering the activation energy for SAM formation. Our dip-coating approach is especially suitable for scale-up in an industrial environment, where speed, environmental friendliness, shape and size of objects to be coated are all important factors to be considered.

After clarifying the OPA SAM formation mechanism and confirming the rapidity of full-coverage formation, we conducted our experiments for the thermal stability study on OPA SAMs dip-coated on Al films using a 1 mM OPA solution in anisole. Shown in Fig. 5 are CAs obtained on OPA/Al samples as a function of annealing temperature. The static CA of the control (*i.e.*, the OPA/Al sample without annealing) plotted in Fig. 5 is 120°, which indicates that the OPA molecules are covalently bonded to the Al film. This is because physically adsorbed OPA molecules would have a much smaller CA as reported previously.[20] CAs remained at the level of 120° on the OPA samples subjected to annealing at temperatures 100 and 150 °C. This experimental observation is a reflection that the molecules are covalently bonded to the surface through P–O–Al linkage[37] for the control and annealed samples.

The CA for the sample annealed at 200 °C becomes 110°, a slight decrease from 120°. For samples annealed in the temperature range of 200–400 °C, CAs decrease from 110° to less than 10°. The results shown in Fig. 5 indicate that the surface of the OPA SAMs becomes hydrophilic upon annealing above 250 °C. There are two possibilities for the observed increased hydrophilicity: (a) the OPA molecules are intact but rearranged to expose the substrate which is hydrophilic, or (b) the bonding between the OPA headgroups and the substrate surface is intact but the OPA methyl groups and/or alkyl chains are oxidized so that the surface of the monolayer starts to have oxygen-containing species leading to increased hydrophilicity. Since OPA molecules are bonded to the Al film *via* covalent bonds (P–O–Al), it is more likely that the oxidation of the alkyl chains is responsible for the increased hydrophilicity of the OPA/Al samples, especially in our case the experiment was conducted in air.

In order to clarify which of the two possibilities described above is responsible for the observed CA variations, we used

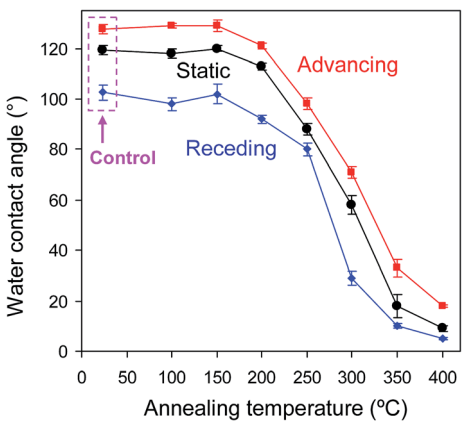

Fig. 5 Water contact angles measured on OPA/Al samples as a function of annealing temperature (100–400 °C). The data for the control are indicated by the box.

TOF-SIMS to follow the observed changes in surface chemistry of our OPA SAMs as a function of annealing temperature. The negative and positive secondary ion mass spectra obtained on the control and OPA samples annealed (in air) at 100–400 °C are shown in Fig. 6 and 7, respectively. For the control, as shown in Fig. 6a, the most abundant negative ion fragments detected from OPA SAMs are C_2H^- (*m*/*z* 25.007), PO_2^- (62.963) and PO_3^- (78.959). With increased annealing temperatures, there are no significant variations in intensities of PO_2^- and PO_3^-, while the intensity of C_2H^- decreases. The most significant changes in the spectra shown in Fig. 6a are increased intensities of O^- (15.991) and OH^- (17.001).

Fig. 6b shows the spectra in the *m*/*z* range covering CN^- (26.010), C_2HO^- (41.003) and CHO_2^- (44.997), all of their intensities increase with increased annealing temperatures. We notice that the intensity of CN^- has increased significantly for samples annealed above 300 °C, which is due to the incorporation of nitrogen from air. CH_2O^- and CHO_2^- are the two major species indicative of oxidation of alkyl chains.[27] These two species are common fragments detected from organic molecules containing carboxylates and esters. Therefore, the observed increase in their intensities suggests that the alkyl chains of the OPA molecules are oxidized upon their annealing at elevated temperatures.

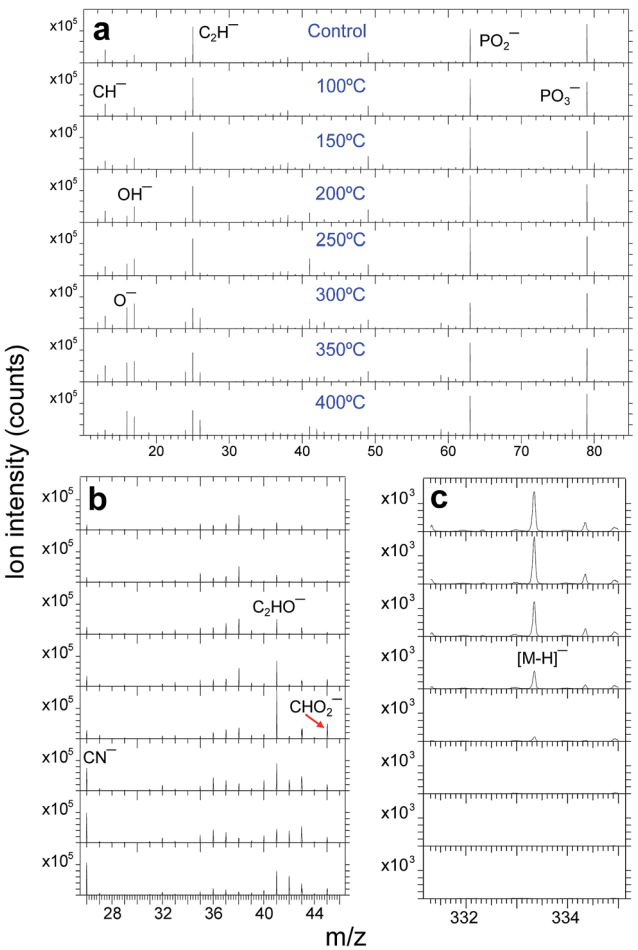

Fig. 6 Negative secondary ion mass spectra obtained on the control and OPA/Al samples annealed in air at temperatures 100–400 °C in *m*/*z* ranges of (a) 10–85, (b) 25–46 and (c) 331–335.

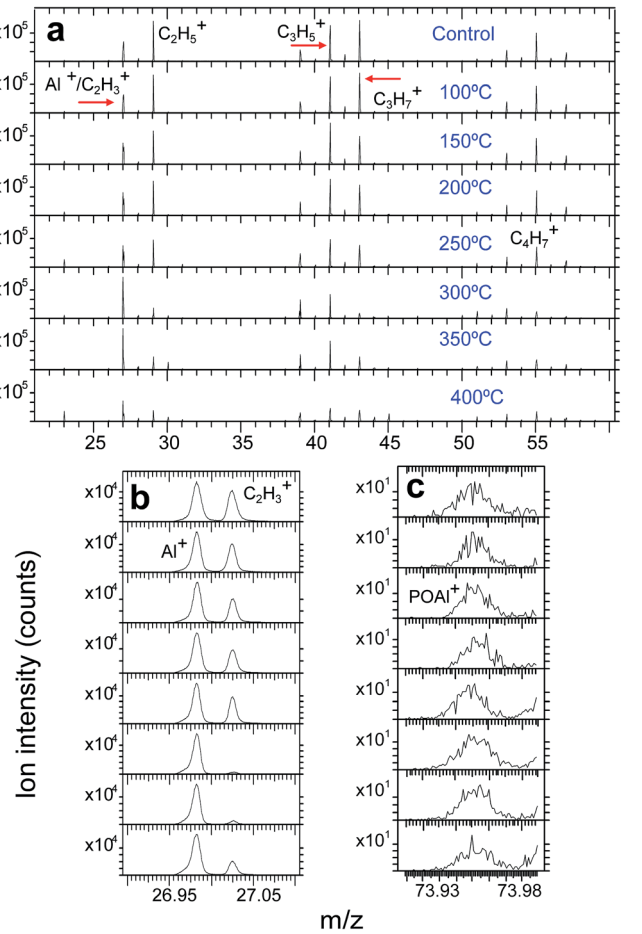

Fig. 7 Positive secondary ion mass spectra obtained on the control and OPA/Al samples annealed at temperatures 100–400 °C in *m*/*z* ranges of (a) 21–60, (b) 26.9–27.1 and (c) 73.9–74.0.

As shown in Fig. 6c, the intensity of the deprotonated molecular ion fragment $[M - H]^-$ or $C_{18}H_{38}PO_3^-$ (333.248), with M representing the OPA molecular formula of $C_{18}H_{39}PO_3$, decreases significantly with increased annealing temperatures and vanishes for samples annealed at 300 °C and above. This observation is a reflection that no OPA molecules could stand for annealing at 300 °C and above. With the increased intensities in O^-, OH^-, CH_2O^- and CHO_2^-, it is clear that OPA molecules are oxidized at these elevated temperatures.

The positive ion mass spectra in Fig. 7a show that the spectrum of the control is dominated by hydrocarbon fragments, such as $C_2H_5^+$ (29.040), $C_3H_5^+$ (41.039), $C_3H_7^+$ (43.054) and $C_4H_7^+$ (55.054). At *m*/*z* 27 are two peaks for Al^+ (26.981) and $C_2H_3^+$ (27.024), which are clearly resolved in Fig. 7b. We notice that there is a drastic decrease in the intensity of $C_2H_3^+$ for the sample annealed at 300 °C, which happens to be the temperature when no intact OPA molecules exist (Fig. 6c). The increased intensity of $C_2H_3^+$ for the samples annealed at 350 and 400 °C hints that there are some chemical compositional changes occurred at these higher temperatures, which remain unclear at

this point. Nevertheless, as shown in Fig. 7a, the ion intensities of the higher mass hydrocarbon species (*e.g.*, $C_2H_5^+$, $C_3H_5^+$, $C_3H_7^+$ and $C_4H_7^+$) decrease at elevated annealing temperatures, suggesting that the alkyl chains of the OPA molecules are damaged by the annealing.

Shown in Fig. 7c are ion mass spectra of $POAl^+$ (73.947), which is characteristic of the covalent bond P–O–Al formed between the OPA headgroup and the Al film. This linkage is a result of the condensation reaction[38,39] between the hydroxyl groups from the OPA headgroup and those from the oxidized Al film. As shown in Fig. 7c, for the $POAl^+$ peak, there are no significant changes at annealing temperatures up to 350 °C, with only a slight decrease at 400 °C. It is important to note that $POAl^+$ is also detected on the control. By combining this TOF-SIMS result and the CA observation in Fig. 5, it is clear that OPA molecules are covalently bonded to the Al film even prior to annealing. However, from these TOF-SIMS and water CA results, we could not determine whether OPA molecules have mono-, bi- or tridentate bonding to the Al film.[40]

In order to extract information in regard to changes of the OPA molecules upon annealing, we plot in Fig. 8 the intensities of PO_2^-, PO_3^-, O^-, C_2HO^-, CHO_2^-, $[M - H]^-$ and $POAl^+$ obtained from the control and samples annealed at temperatures 100–400 °C. It is clear that upon annealing there are no significant changes in intensities of PO_2^- and PO_3^-. These two ion fragments are characteristic of the OPA molecular headgroup, but not the OPA molecule. Therefore, these two ion fragments are not informative in studying alterations of molecules upon annealing. Nonetheless, their behavior does indicate that the phosphate groups remained largely unchanged on the substrate even after they were annealed at 400 °C.

$[M - H]^-$ is a sensitive marker for studying intact OPA molecules since an altered OPA molecule no longer contribute to the generation of a deprotonated molecular ion.[27] As shown in Fig. 8, there are no significant changes seen in the intensity of $[M - H]^-$ for OPA/Al samples annealed at temperatures up to 150 °C. This is a reflection that the annealing has no impact on the molecules, which is in agreement with the unchanged CAs measured on these samples (Fig. 5). For the sample annealed at 200 °C, the intensity of $[M - H]^-$ decreases to approximately 80% of that of the control. This indicates that some of the molecules have been altered by the annealing. This explains the CA measured on this sample, which is only a decrease of ~10° from that of the control and the samples annealed at 100 and 150 °C. When the annealing temperature reaches 250 °C, the intensity of $[M - H]^-$ decreases significantly, retaining only 10% of that of the control. When the annealing temperatures are raised to 300 °C and above, no $[M - H]^-$ fragment is detectable, which is proof that no intact OPA molecules remained. The CAs measured on these samples decrease significantly, indicating that the surface becomes hydrophilic.

By carefully investigating the mass spectra as a function of annealing temperature, we have identified species useful in revealing oxidation of the alkyl chains of OPA molecules. These are O^-, C_2HO^- and CHO_2^-. O^- shows an increase by one order of magnitude when the annealing temperature is 300 °C and above, where no intact OPA molecules exist. It is worth noting that there is a peak in the intensity *vs.* annealing temperature curve at 250 °C for intensities of C_2HO^- and CHO_2^-. We explain this observation by considering oxidation of alkyl chains of OPA molecules as follows. At temperatures lower than 250 °C, more and more C–H bonds are oxidized with increased temperatures, resulting in increased intensities for C_2HO^- and CHO_2^-. However, with the annealing temperatures becoming higher and higher, the oxidized hydrocarbons will also have more chance to be removed as volatile species of H_2O and CO_2, causing a reduction of C_2HO^- and CHO_2^-. These two competing processes shall be responsible for the observed peaks at 250 °C for C_2HO^- and CHO_2^-. In order to make sure that this observation about the peaks and their positions in the intensity *vs.* temperature relationship is reproducible, we repeated the TOF-SIMS experiment by running another set of samples and obtained very similar results to those shown in Fig. 8, not only for the profiles of C_2HO^- and CHO_2^-, but also for all other species.

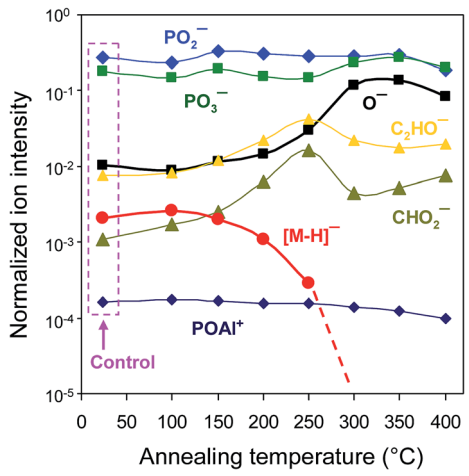

Fig. 8 Normalized ion intensities as a function of annealing temperature. The data for the control (*i.e.*, without annealing), indicated by the box, are also plotted. The standard deviations for all data are up to several percent (not shown). Because there is no longer a peak corresponding to the deprotonated molecular ion fragment $[M - H]^-$ upon annealing at 300 °C and above, the broken line serves to guide the eye to the decreasing trend of $[M - H]^-$.

4. Conclusions

We have developed a dip-coating approach for preparing OPA SAMs on hydrophilic substrates with the use of anisole, a nonpolar solvent that has a dielectric constant of 4.3 and is more environmentally friendly in comparison with chlorine-containing solvents having a similar dielectric constant, such as chloroform and trichloroethylene. The concentration of the polar OPA headgroups on the medium surface is responsible for such a quick formation of monolayers on a hydrophilic surface: the dipping time is only a couple of seconds and no rinse is needed. Since dip-coating is the easiest way to handle objects having a wide variety of shapes and sizes, this method can be readily integrated into product lines for products where OPA

SAMs add value to surface modification. Moreover, this approach is environmentally friendly because there is no waste of chemicals, compared to other mass-production approaches such as painting and spraying.

With the two surface-sensitive techniques of water contact angle and TOF-SIMS, we clarified that the hydrophobicity of OPA SAMs dip-coated on an Al film is maintained upon annealing in air at temperatures up to 200 °C, even though a small portion of the alkyl chains of OPA molecules are oxidized at this temperature. TOF-SIMS investigation revealed that the degradation mechanism for the OPA SAMs annealed above 200 °C is dominated by oxidation of the alkyl chains, rather than the break-up of the covalent bond between the OPA headgroup and the Al film. Therefore, the thermal stability of the OPA/Al system in air is limited by oxidation of alkyl chains. Our results suggest the utility of the OPA/Al system in applications (such as organic electronic devices) where heat treatment at temperatures up to 200 °C may be imposed.

Acknowledgements

This work was supported in part by a University Partnership Committee Funded Research contract from Xerox Research Centre of Canada and a Collaborative Research & Development grant from the Natural Sciences and Engineering Research Council of Canada.

References

1 A. Ulman, *Chem. Rev.*, 1996, **96**, 1533.
2 F. Schreiber, *Prog. Surf. Sci.*, 2000, **65**, 151.
3 J. C. Love, L. A. Estroff, J. K. Kriebel, R. G. Nuzzo and G. M. Whitesides, *Chem. Rev.*, 2005, **105**, 1103.
4 D. K. Schwartz, *Annu. Rev. Phys. Chem.*, 2001, **52**, 107.
5 I. L. Liakos, R. C. Newman, E. McAlpine and M. R. Alexander, *Langmuir*, 2007, **23**, 995.
6 R. Luschtinetz, A. F. Oliveira, J. Frenzel, J.-O. Joswig, G. Seifert and H. A. Duarte, *Surf. Sci.*, 2008, **602**, 1347.
7 C. Queffelec, M. Petit, P. Janvier, D. A. Knight and B. Bujoli, *Chem. Rev.*, 2012, **112**, 3777.
8 G. Guerrero, J. G. Alauzun, M. Granier, D. Laurencin and P. H. Mutin, *Dalton Trans.*, 2013, **42**, 12569.
9 R. C. Longo, K. J. Cho, W. G. Schmidt, Y. J. Chabal and P. Thissen, *Adv. Mater.*, 2013, **23**, 3471.
10 A. Bora, A. Pathak, K.-C. Liao, M. I. Vexler, A. Kuligk, A. Cattani-Scholz, B. Meinerzhagen, G. Abstreiter, J. Schwartz and M. Tornow, *Appl. Phys. Lett.*, 2013, **102**, 241602.
11 Y. Ito, A. A. Virkar, S. Mannsfeld, J. H. Oh, M. Toney, J. Locklin and Z. N. Bao, *J. Am. Chem. Soc.*, 2009, **131**, 9396.
12 U. Zschieschang, T. Yamamoto, K. Takimiya, H. Kuwabara, M. Ikeda, T. Sekitani, T. Someya and H. Klauk, *Adv. Mater.*, 2011, **23**, 654.
13 B. M. Dhar, R. Özgün, T. Dawidczyk, A. Andreou and H. E. Katz, *Mater. Sci. Eng., R*, 2011, **72**, 49.
14 O. Acton, M. Dubey, T. Weidner, K. M. O'Malley, T.-W. Kim, G. G. Ting, D. Hutchins, J. E. Baio, T. C. Lovejoy, A. H. Gage, D. G. Castner, H. Ma and A. K.-Y. Jen, *Adv. Funct. Mater.*, 2011, **21**, 1476.
15 O. Acton, D. Hutchins, L. Árnadóttir, T. Weidner, N. Cernetic, G. G. Ting, T.-W. Kim, D. G. Castner, H. Ma and A. K.-Y. Jen, *Adv. Mater.*, 2011, **23**, 1899.
16 F. S. M. Hashemi, C. Prasittichai and S. F. Bent, *J. Phys. Chem. C*, 2014, **118**, 10957.
17 D. J. Beesley, J. Semple, L. K. Jagadamma, A. Amassian, M. A. McLachlan, T. D. Anthopoulos and J. C. deMello, *Nat. Commun.*, 2014, **5**, 3933.
18 J. T. Woodward, A. Ulman and D. K. Schwartz, *Langmuir*, 1996, **12**, 3626.
19 S. P. Pujari, L. Scheres, A. T. M. marcelis and H. Zuilhof, *Angew. Chem., Int. Ed.*, 2014, **53**, 6322.
20 H.-Y. Nie, M. J. Walzak and N. S. McIntyre, *J. Phys. Chem. B*, 2006, **110**, 21101.
21 J. S. Jaworski, M. Cembor and M. Orlik, *J. Electroanal. Chem.*, 2005, **582**, 165.
22 R. J. Good, *J. Adhes. Sci. Technol.*, 1992, **6**, 1269.
23 A. Benninghoven, *Angew. Chem., Int. Ed. Engl.*, 1994, **33**, 1023.
24 S. Muramoto, J. Brison and D. G. Castner, *Anal. Chem.*, 2012, **84**, 365.
25 K. V. Wolf, D. A. Cole and S. L. Bernasek, *Anal. Chem.*, 2002, **74**, 5009.
26 N. Winograd and B. Garrison, *Int. J. Mass Spectrom.*, 2001, **212**, 467.
27 H.-Y. Nie, *Anal. Methods*, 2013, **5**, 4911.
28 J. S. Fletcher, N. P. Lockyer, S. Vaidyanathan and J. C. Vickerman, *Anal. Chem.*, 2007, **79**, 2199.
29 T. Stephan, J. Zehnpfenning and A. Benninghoven, *J. Vac. Sci. Technol., A*, 1994, **12**, 405.
30 H. B. Eral, D. J. C. M. 't Mannetje and J. M. Oh, *Colloid Polym. Sci.*, 2013, **291**, 247.
31 L. C. Gao and T. J. McCarthy, *Langmuir*, 2006, **22**, 6234.
32 N. Belman, K. J. Jin, Y. Golan, J. N. Israelachvili and N. S. Pesika, *Langmuir*, 2012, **28**, 14609.
33 R. M. Linford, P. Fenter, P. M. Eisenberger and C. E. D. Chidsey, *J. Am. Chem. Soc.*, 1995, **117**, 3145.
34 A. V. Marenich, C. J. Cramer and D. G. Truhlar, *J. Phys. Chem. B*, 2009, **113**, 6378.
35 N. J. O'Reilly and E. Magner, *Langmuir*, 2005, **21**, 1009.
36 D. K. Schwartz, *Surf. Sci. Rep.*, 1997, **27**, 241.
37 H.-Y. Nie, *Anal. Chem.*, 2010, **82**, 3371.
38 P. H. Mutin, G. Guerrero and A. J. Vioux, *Mater. Chem.*, 2005, **15**, 3761.
39 M. J. Pellerite, T. D. Dunbar, L. D. Boardman and E. J. Wood, *J. Phys. Chem. B*, 2003, **107**, 11726.
40 A. Bulusu, S. A. Paniagua, B. A. MacLeod, A. K. Sigdel, J. J. Berry, D. C. Olson, S. R. Marder and S. Graham, *Langmuir*, 2013, **29**, 3935.

